lowing term should be added to Eq. (16):

$$(A_{24}-A_{42})\left[\frac{7\sqrt{15}}{16}G_2^{24}(\cos^2\theta-\cos^4\theta)+\left(\tfrac{21}{2}(\tfrac{5}{6})^{1/2}G_1^{24}-\frac{7\sqrt{15}}{16}G_2^{24}\right)\cos^6\vartheta\cos^2\phi\sin^2\phi\right]\times(\cos^2\phi-\sin^2\phi)\,.$$

[18]C. T. Alonso, Ph.D. thesis, Massachusetts Institute of Technology, 1970 (unpublished).
[19]R. V. Pound, Phys. Rev. 79, 685 (1950).
[20]N. J. Leisi, in *Angular Correlations in Nuclear Disintegration* (see Ref. 2).
[21]O. C. Kistner, A. W. Sunyar, and P. Thieberger, Bull. Am. Phys. Soc. 16, 80 (1971).
[22]R. M. Steffen and H. Frauenfelder, in *Perturbed Angular Correlations*, edited by E. Karlsson, E. Matthias, and K. Siegbahn (see Ref. 14), pp. 4, 20.

PHYSICAL REVIEW C VOLUME 5, NUMBER 3 MARCH 1972

Reaction ^{9}Be$(\alpha,n)^{12}$C from 1.7 to 6.4 MeV*

A. W. Obst,† T. B. Grandy,‡ and J. L. Weil§
Department of Physics, University of Kentucky, Lexington, Kentucky 40506

(Received 25 June 1971)

The 0° excitation functions for the reaction ^{9}Be$(\alpha,n)^{12}$C leading to the ground and first excited states of ^{12}C were measured between 1.69- and 6.44-MeV bombarding energy, while those for the second- and third-excited-state neutron groups were measured above 2.94- and 5.94-MeV bombarding energy, respectively. Angular distributions of the ground state and first two excited-state neutron groups were measured at 17 bombarding energies between 3.21 and 6.44 MeV, and for the third-excited-state neutron group they were measured at 6.24- and 6.44-MeV bombarding energy. The magnitude of the cross sections for the ground- and first-excited-state neutron groups agrees well with the larger of the two sets of conflicting magnitudes reported in the literature. Double-differential cross sections of the continuum of low-energy neutrons were measured as a function of angle and neutron energy for 10 bombarding energies ranging from 4.86 to 6.44 MeV. The features of the continuum are consistent with the sequential decay $^9\text{Be}+\alpha\rightarrow{}^9\text{Be}^*+\alpha'\rightarrow{}^8\text{Be}+n+\alpha'$, proceeding through the 1.67-, 2.43-, and 3.04-MeV excited states in ^{9}Be. The ratio of the populations of the first and second excited states in the ^{9}Be$(\alpha,n)^{12}$C reaction was determined at 16 bombarding energies between 3.99 and 6.44 MeV.

I. INTRODUCTION

The reaction ^{9}Be$(\alpha, n)^{12}$C produces neutron groups with discrete energies corresponding to the low-lying levels shown in the energy level diagram[1] for ^{12}C in Fig. 1. In the bombarding energy range up to $E_\alpha = 6$ MeV conflicting measurements of the absolute magnitudes of the cross sections for the various neutron groups from this reaction have been reported. The absolute cross sections of Retz-Schmidt *et al.*[2] and of Van der Zwan and Geiger[3] agree with the total cross-section measurement of Gibbons and Macklin[4] and also with the measurement of Ajzenberg-Selove and Stelson.[5] However, the measured cross sections of Bonner *et al.*,[6] Risser, Price, and Class,[7] and Miller and Kavanagh[8] agree with each other but are smaller in magnitude than the cross sections of Refs. 2–5 by approximately a factor of 2. On the other hand, the shapes of the angle-integrated cross sections, 0° excitation functions, and angular distributions of the neutron groups populating the ground and first excited states of ^{12}C from these two sets of experiments agree well with each other in the energy range of the present experiment.

One purpose of the present experiment was to measure the absolute cross sections of the neutron groups populating ^{12}C in an attempt to resolve the discrepancy between the two sets of data, and thus to determine the usefulness of the high-energy neutron group as a source of neutrons for neutron-scattering experiments in the energy range between 9 and 14 MeV. To this end, excitation functions at 0° of all neutrons with energies above 0.5 MeV were measured between 1.7- and 6.4-MeV bombarding energy. Angular distributions of these neutrons were measured at 17 bombarding energies between 3.2- and 6.4-MeV bombarding energy.

A second purpose was to measure the cross sections of the groups populating the higher excited states of ^{12}C. Except for the recent work of Van der Zwan and Geiger,[3] no absolute cross-

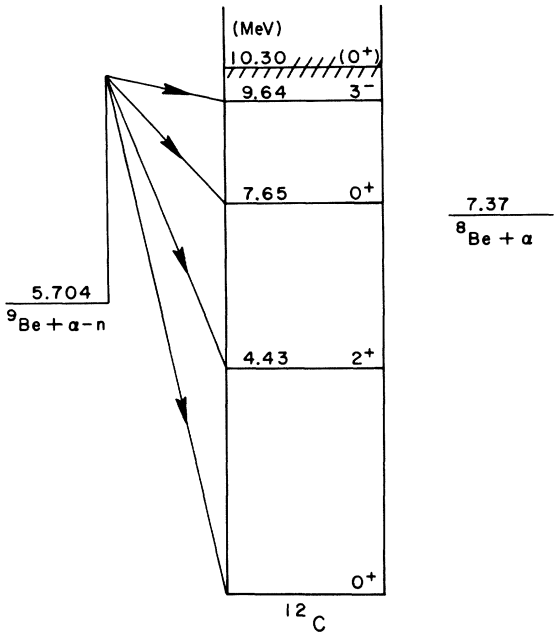

FIG. 1. Energy-level diagram for ^{12}C.

section measurements have been previously reported on the n_2 group below 6 MeV[9] or on the n_3 group below 9.8-MeV bombarding energy. Differential cross sections for the n_2 group, which populated the 7.653-MeV level in ^{12}C, were measured in the present experiment in the bombarding energy range from 3.2 to 6.4 MeV, and for the n_3 group, which populates the 9.638-MeV level in ^{12}C, differential cross sections were measured for the bombarding energies of 6.24 and 6.44 MeV. In addition, double-differential cross sections as functions of angle and neutron energy for the continuum of low-energy neutrons seen at neutron energies below those of the n_2 group were measured at 10 energies above a bombarding energy of 4.8 MeV. The only previous work at these energies on these continuum neutrons is that of St. Romain *et al.*[10]

The ratio R of the angle-integrated yields for the n_1 and n_2 neutron groups was determined from the present measurements at the 16 bombarding energies where complete angular distributions were measured. This ratio is of interest in determining the probability of formation of ^{12}C in the red giant stars by the resonance reaction $3\alpha \rightarrow {}^{12}C^{*}(7.653) \rightarrow {}^{12}C(\text{g.s.})$. Alburger[11] found the probability of direct decay of $^{12}C^{*}(7.653)$ to the ground state using the reaction $^{9}Be(\alpha, n)^{12}C$. His conclusions required the knowledge of the ratio R, which was approximately known[5,11] at the time. The present determination of R reduces the error in the ratio from ±12% to ±5%.

II. EXPERIMENTAL PROCEDURE

A. Experimental Apparatus

The present measurements were made using the time-of-flight technique. Singly charged helium ions from the University of Kentucky model CN Van de Graaff accelerator were used to bombard

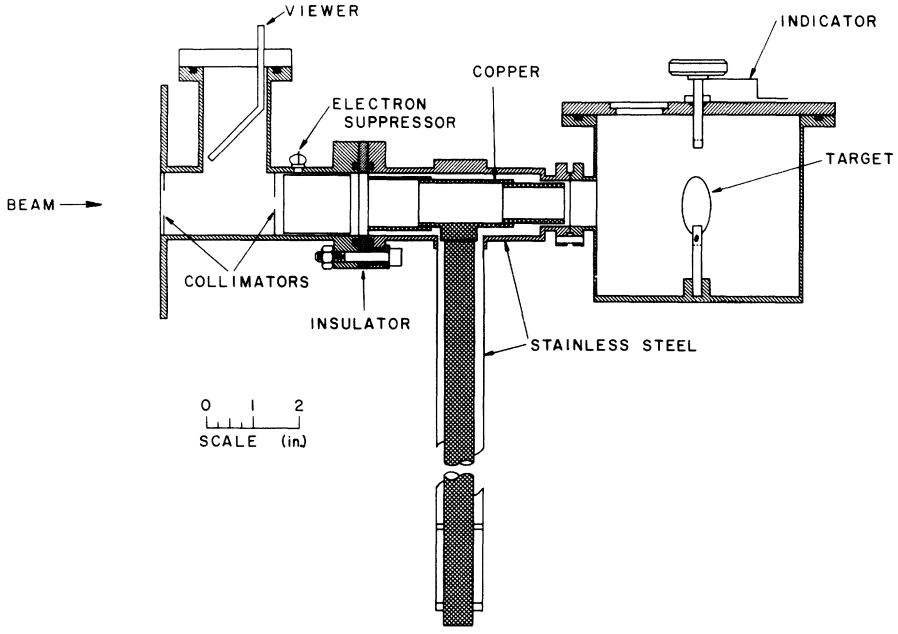

FIG. 2. Target chamber with cold trap to prevent buildup of carbon on the target.

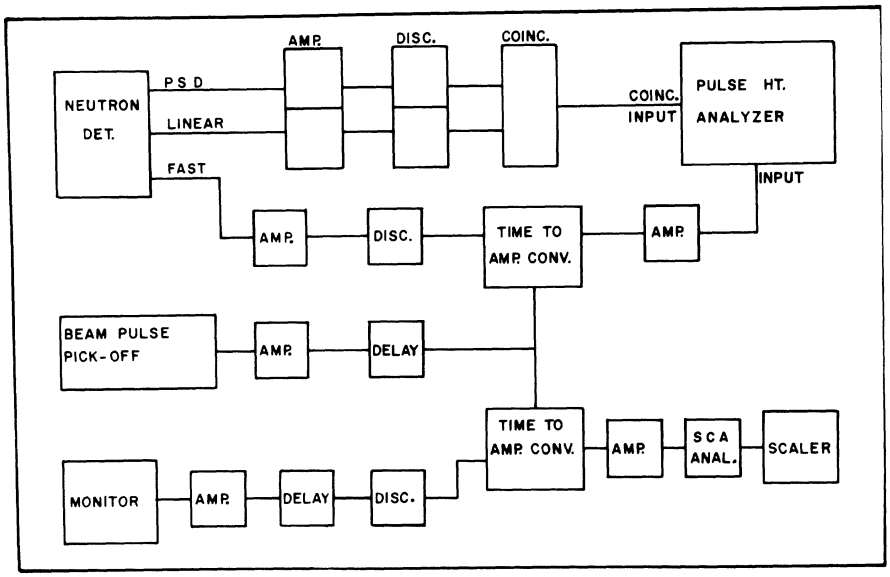

FIG. 3. Block diagram of time-of-flight electronics used in the experiment.

a thin evaporated target of beryllium. Terminal pulsing provided beam bursts of about 14-nsec duration and a Mobley bunching system reduced the pulse length to less than 2 nsec. The energy calibration of the analyzing magnet was determined by measuring thresholds for the reactions[12] ^{7}Li(p, n)^{7}Be and ^{27}Al(p, n)^{27}Si with both atomic and molecular hydrogen beams.

Beryllium targets were prepared by resistive heating of beryllium chips in a tantalum boat. The beryllium was evaporated onto 0.02-in.-thick tantalum disks. The target was mounted inside a cylindrical target chamber shown in Fig. 2. A hollow cylindrical cold trap coaxial with the beam can also be seen in Fig. 2. It consists of a copper cylinder mounted on the top of a copper rod whose bottom end projects into a Dewar of liquid nitrogen. This trap inhibits carbon deposits from the cracking of hydrocarbons onto the target which would cause an unknown shift in the mean α energy. Lack of this precaution in earlier measurements[2] caused energy shifts as large as 100 keV.

The shape of the 0° excitation functions were measured using current integration for cross-section normalization. The normalization during the measurement of the angular distributions was also checked by an independent neutron monitor time-of-flight detector located 1 m above the target. The agreement between these two methods of relative normalization was found to be 5% or better, and gives an estimate of the maximum target nonuniformity. The beam current used in the present measurements was kept at 1–2 μA, since larger beam currents tended to erode the targets. The counting rates under these conditions caused dead

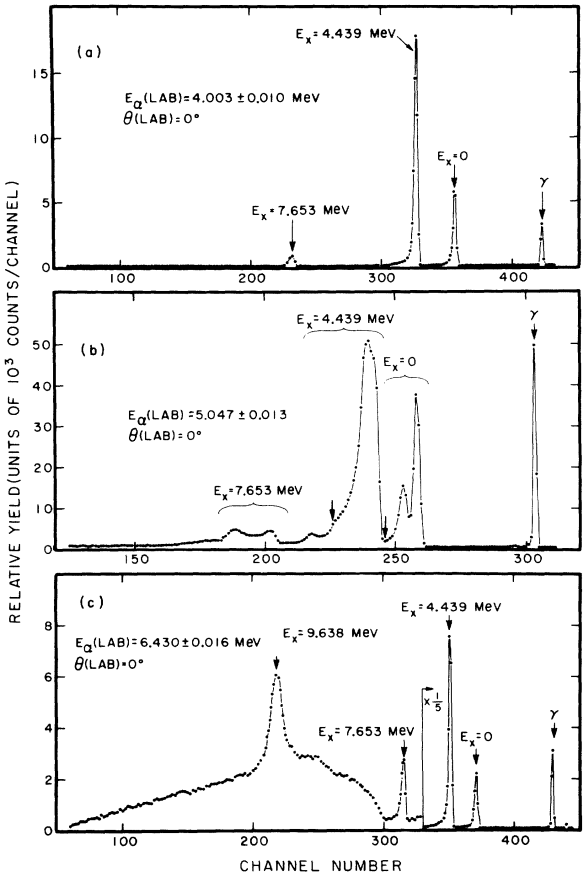

FIG. 4. (a) ^{9}Be(α,n)^{12}C time-of-flight spectrum at E_α =4.00 MeV using a thin target. (b) ^{9}Be(α,n)^{12}C time-of-flight spectrum at E_α =5.05 MeV using a thick target (see Sec. II C). (c) ^{9}Be(α,n)^{12}C time-of-flight spectrum at E_α =6.43 MeV using a thin target.

times of 10% or less, for which corrections were made.

The main detector consisted of a 5-in.×5-in. NE213 cylindrical encapsulated liquid scintillator coupled to an XP1040 photomultiplier tube and mounted at a distance of 3.7 m from the target in a neutron shield[13] moving on a circular track. The circular beam collimators allowed a 2° maximum spread in the incident beam, while the circular profile of the detector subtended a maximum angle of 1.7°. The effective over-all angular spread was about 2°.

Standard time-of-flight techniques were used on the main detector and included γ-ray elimination by pulse-shape discrimination (PSD). A block diagram of the time-of-flight electronics is shown in Fig. 3. An energy discriminator on the main detector was set at $\frac{1}{3}$ the pulse height of the 60-keV γ-ray peak from ^{241}Am, corresponding to a neutron energy of about 0.16 MeV. The output signal of the energy discriminator, in coincidence with the γ-ray discriminator, provided a gating signal for the multichannel analyzer which stored the time spectra. Several typical time spectra are shown in Fig. 4. The monitor electronics were similar to those of the main detector except that no energy or γ-ray discrimination was used. The monitor counts were fed to a single-channel analyzer (SCA) whose window was set on the n_0 and n_1 neutron peaks together and whose output was stored in a scaler.

B. Efficiency of Detector

The energy dependence and absolute value of the neutron-detection efficiency of the main detector were determined by measuring yields for the reactions $D(d,n)^3He$ and $T(p,n)^3He$ which have known cross sections.[14,15] The $D(d,n)^3He$ 0° excitation function measured with a gas-cell target covered the neutron energy range from 4.7 to 9.1 MeV. A measurement of the $D(d,n)^3He$ angular distributions at $E_d = 1.96$ MeV was used to study neutrons between 3.0 and 4.7 MeV. The above measurements were made under one set of collimator and beam conditions and the results are shown in Fig. 5 and are summarized by the lower dashed line. The efficiency obtained from an angular-distribution measurement at $E_d = 5.80$ MeV, mostly under different collimator and beam conditions is also shown in Fig. 5 and is summarized by the upper dashed line.

The low-energy portion of the efficiency curve was determined from relative $T(p,n)^3He$ angular-distribution measurements at $E_p = 2.25$ and 4.70 MeV which were normalized to a weighted average of the two $D(d,n)^3He$ curves. The region from 9-

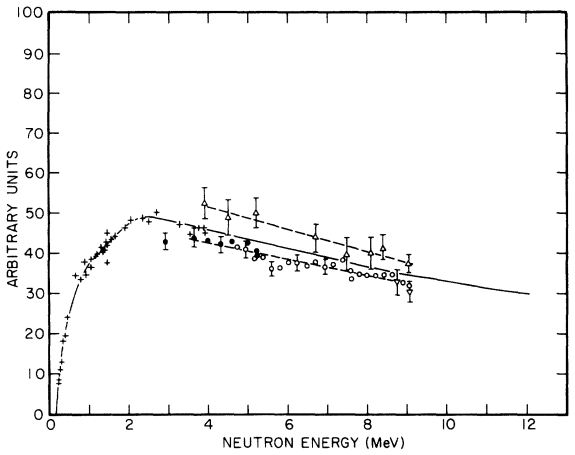

FIG. 5. Relative neutron-detection efficiency of 5-in. ×5-in. detector. The $D(d,n)^3He$ data of Set I taken under one set of beam and collimator conditions include the results from a 0° excitation function (○) and angular distributions at 1.96 MeV (●) and 5.80 MeV (▽). The $D(d,n)^3He$ data of Set II taken under different beam and collimator conditions consist of an angular-distribution measurement at 5.80 MeV (△). The $T(p,n)^3He$ data (+) consist of relative angular-distribution measurements taken at bombarding energies of 2.25 and 4.70 MeV.

to 12-MeV neutron energy was extrapolated from the average $D(d,n)^3He$ curve by normalizing the Monte Carlo calculations of Verbinski *et al.*[16] to the average measured efficiency curve. The efficiency is shown in Fig. 5, but only in relative units, since the same detector, geometry, and current integrator were used to measure both the efficiency and the data, and, hence, those factors canceled out in the calculation of the absolute magnitude of the $^{9}Be(\alpha,n)^{12}C$ cross section.

The data taking was completed over a period of 4 months during which the efficiency was checked on each 3- or 4-day run by repeating a $^{9}Be(\alpha,n)^{12}C$ angular distribution at 4.2-MeV bombarding energy with a given beryllium target. The energies of the three neutron groups from this reaction vary with angle from 0.4 to 9.8 MeV at this bombarding energy, which covers most of the efficiency curve. The absolute detector efficiency checked in this way always agreed with the previously measured efficiency to within 5%.

C. Target-Thickness Determination

The target-thickness was found by weighing the thin targets and also by a comparison method using a thick beryllium target. The targets were evaporated in pairs and the weights of the two members of each pair were found to agree to better than the accuracy of the weighing, which was ±10%. Relative neutron yields of the various tar-

gets were measured at a given energy. The weights were then adjusted so that they were in direct proportion to the neutron yields from targets made in different evaporations. The amount of adjustment for each target was about 10%, which was within the weighing accuracy.

In the thick-target comparison method the time spectrum [Fig. 4 (b)] from a target infinitely thick to α particles was measured at a given bombarding energy with the same neutron-detection system used for the rest of this work. The yield of a neutron group in the spectrum was integrated between the maximum energy of the group and a lower-energy point which could be identified with the corresponding point on the 0° excitation function. These points are indicated by broad arrows on Figs. 4(b) and 6. The yield of a group was corrected for 6% attenuation through the thick beryllium target and designated as Y_{thick}.

The region of the thin-target yield curve (with the detector efficiency still folded in) between the thick-target bombarding energy and the lower-energy point was divided into 50 energy intervals, each of which corresponded to the α-particle-energy loss in a fictitious target with surface density N_Δ μg/cm^2. The value of N_Δ was $\frac{1}{50}$ of the integral of the reciprocal of a quadratic fit to dE/dx for beryllium[17] over the energy range for which Y_{thick} was calculated.

The yield values of the midpoints of the 50 energy intervals in the thin-target yield curve were summed and this sum is Y_{thin}. The thickness of the thin target is then given by

$$N_{\text{thin}} = N_\Delta \frac{Y_{\text{thin}}}{Y_{\text{thick}}} .$$

Three thick-target spectra were measured at 5-MeV bombarding energy and one at 6 MeV. Using both the n_0 and n_1 groups in each spectrum provided eight estimates of the target thickness. The deviations among the nine values, including that by weighing, were less than 10%. The value used in calculating absolute cross sections was the weighted mean of all nine measurements and was determined to be 37.2 ± 1.9 μg/cm^2. This corresponds to an energy loss in the target by the α particles of 56 keV at 1.7-MeV bombarding energy and 23 keV at 6.4 MeV.

D. Error Analysis

The relative error in the cross sections for the discrete neutron groups depends on target nonuniformity, counting statistics, variations in current integration, and the relative error in detector efficiency. The error due to uncertainty in the efficiency over the span of an excitation function of a single group or of an angular distribution is less

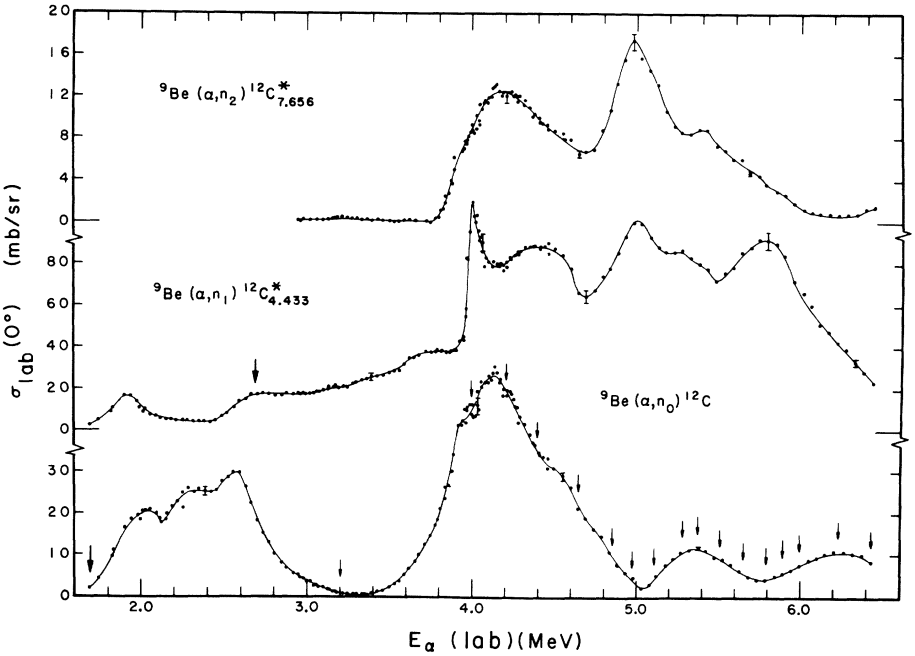

FIG. 6. ^{9}Be(α,n)^{12}C 0° excitation functions for the first three levels in ^{12}C. The smooth lines drawn through the data are visual aids only. The small arrows indicate the bombarding energies at which angular distributions were measured. Typical relative errors are shown. The large arrows indicate the low-energy limits for the yield sum in the thin-to-thick target comparison (see Sec. II C).

than ±5%, since the relative error over the entire efficiency curve between 0.5- and 12-MeV neutron energy is estimated to be about ±7%. The error due to target nonuniformity is ±5% as discussed in Sec. II A, while the relative error in current integration is ±2%. Including statistical errors, which were less than 1% most of the time, the relative errors in the $^{9}Be(\alpha,n)^{12}C$ cross sections to the levels in ^{12}C are between ±5 and ±10%. From an estimated error of ±5% in the absolute target thickness and ±9% in the absolute value of the efficiency, we obtain a standard deviation in the absolute normalization of the cross sections for the reaction $^{9}Be(\alpha,n)^{12}C$ leading to the states in ^{12}C of ±10%.

The mean α bombarding energies were determined from the magnet calibration and the reproducibility of resonance energies to have an accuracy of about ±10 keV at low bombarding energies and about ±15 keV at high bombarding energies. The error in angle due to uncertainty in the beam direction after passing through the buncher was ±1°.

The errors in the low-energy $^{9}Be + \alpha$ neutron continuum cross sections were found in the same manner as for the discrete groups. The range of relative errors in the continuum cross sections for a given spectrum is from ±11 to ±50% at the lowest bombarding energy and from ±2 to ±30% at the highest bombarding energy. The largest statistical errors occur near the maximum neutron energies (Figs. 17–22) where the yield becomes small. The relative errors of data points at different angles also include the errors due to nonuniformity of the target (±5%) and to current integration (±2%). These relative errors range from ±11 to ±50% at the lowest bombarding energy down to ±6 to ±30% at the highest bombarding energies. The standard deviation in the absolute normalization of the cross sections for the $^{9}Be(\alpha,n)^{12}C$ low-energy neutron continuum is about ±10%, as for the discrete groups discussed above.

The statistical error at a particular outgoing neutron energy in the continuum was taken to be that for the total yield in the energy-averaging interval (see Sec. IV B) at that particular neutron energy. The large statistical errors implied above are due to the small continuum yields per channel, since good counting statistics in the present experiment were sought only for the discrete neutron groups.

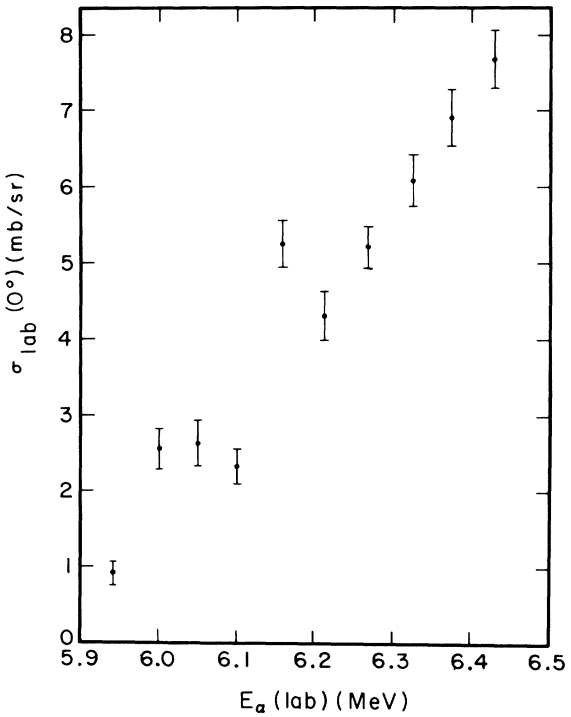

FIG. 7. $^{9}Be(\alpha,n_3)^{12}C^{*}_{9.638}$ excitation function at 0°. Relative errors are shown.

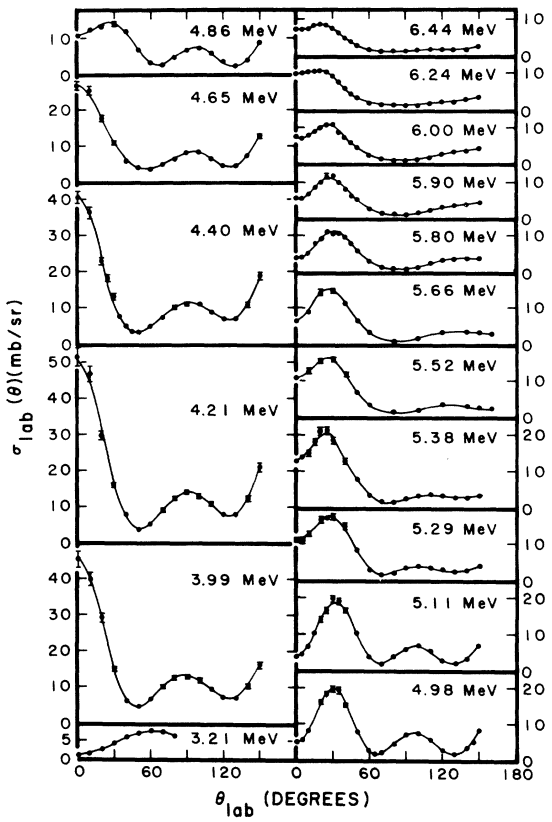

FIG. 8. $^{9}Be(\alpha,n_0)^{12}C$ angular distributions. The smooth curves are center-of-mass Legendre-polynomial fits to the data converted back to the laboratory system. Relative errors are shown when larger than the data points.

III. RESULTS: RESOLVED GROUPS

A. 0° Excitation Functions

The 0° excitation functions are shown in Fig. 6 for the n_0, n_1, and n_2 neutron groups for E_α ranging from 1.7 to 6.4 MeV. The n_0 and n_1 excitation functions agree in magnitude and shape to within 10% with the data of Retz-Schmidt *et al.*[2] and of Van der Zwan and Geiger.[3] The agreement with the only other published data on the n_2 group, that of Van der Zwan and Geiger,[3] is as good except for a discrepancy in magnitude in the region of the first maximum at 4.2-MeV bombarding energy where the present 0° cross section is 40% smaller and also at the second minimum at about 6.0 MeV where the present 0° cross section is 50% smaller. The present cross sections also agree in shape with the data of Risser, Price, and Class[7] but are larger in magnitude by approximately a factor of 2.

The energy regions around 2 and 4 MeV were further investigated with a target 2.5 keV thick at $E_\alpha = 3$ MeV, corresponding to a total energy spread, including that due to the buncher, of less than 8 keV. The purpose of this was to determine whether any fine structure could be further resolved in the ground-state-group excitation function at the shoulder at 4.0 MeV and in the region from 2.00 to 2.18 MeV. No fine structure outside of statistical fluctuations was observed in either energy region. The full width at half maximum of the 3.98-MeV resonance in the n_1 group was measured to be 45 ± 7 keV in this high-resolution work.

The n_2 excitation function at 0° can be seen in Fig. 6 above 3-MeV bombarding energy. The threshold for neutrons to the second excited state of ^{12}C is $E_\alpha = 2.81$ MeV. The n_3 neutron group has its threshold at $E_\alpha = 5.65$ MeV and was observed above 6-MeV bombarding energy, riding on the low-energy continuum as seen in Fig. 4(c). The 0° excitation function for the n_3 group is shown in Fig. 7.

B. Angular Distributions

The angular distributions of the four neutron groups are shown in Figs. 8 through 11, respectively.[18] At most of the bombarding energies the n_0 and n_2 groups have a forward peak at about the same angle. This similarity in shape is probably related to the fact that both final levels in the residual ^{12}C nucleus have $J^\pi = 0^-$. The n_1 group (2^+ level in ^{12}C) varies least rapidly in shape with

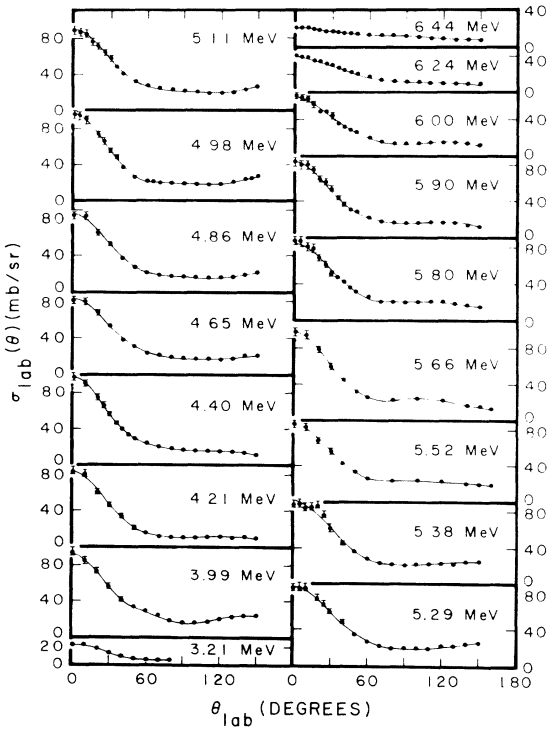

FIG. 9. ^{9}Be$(\alpha, n_1)^{12}$C$^*_{4.439}$ angular distributions (see caption of Fig. 8).

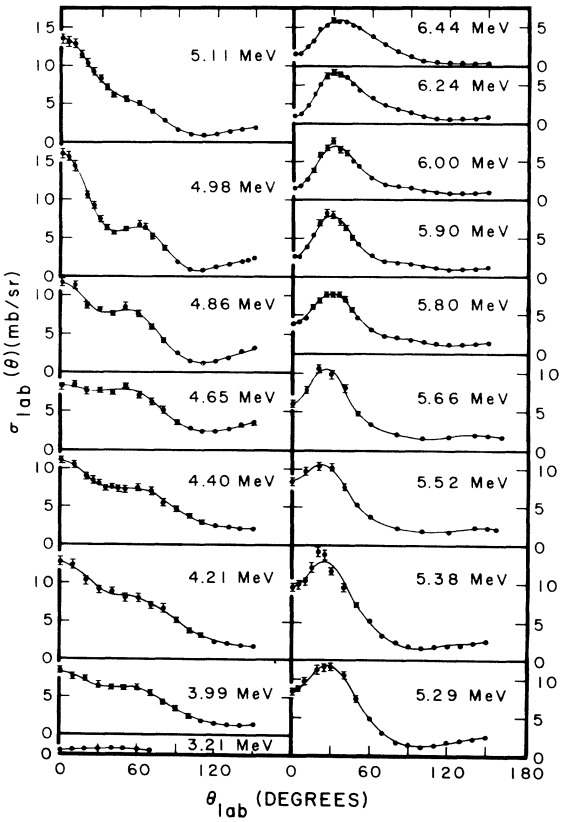

FIG. 10. ^{9}Be$(\alpha, n_2)^{12}$C$^*_{7.656}$ angular distributions (see caption of Fig. 8).

bombarding energy. The n_0 and n_1 differential cross sections in the present experiment agree to better than 10% with the measurements of Retz-Schmidt *et al.*[2] and Van der Zwan and Geiger[3] in shape and magnitude where data were taken at similar bombarding energies, and agree in shape only with the measurements of Risser, Price, and Class.[7] The n_2 angular distributions agree in shape with the measurements of Van der Zwan and Geiger[3] and also with the relative measurements of Gale and Garg.[19]

C. Neutron Groups Integrated Over Angle

The angle-integrated cross sections obtained in the present experiment for the n_0 and n_1 neutron groups agree to better than 10% with the data of Retz-Schmidt *et al.*[2] and with that of Van der Zwan and Geiger.[3] However, the evaluation of Van der Zwan and Geiger[3] for the n_2 group deviates by as much as 50% at some energies from the present work, probably due to their assumption of a constant angular distribution in the α-energy range where no n_2 data were then available.

The reciprocity theorem was used to obtain cross sections for the reaction $^{12}C(n, \alpha_0)^9Be$ from the present data and that of Retz-Schmidt *et al.*[2] and Van der Zwan and Geiger.[3] The results are presented in Fig. 12. Verbinski *et al.*[20] found agreement with the experimental value of the measured $^{12}C(n, \alpha_0)^9Be$ cross section at 14.1 MeV.[21] The only set of measurements reported on the reaction $^{12}C(n, \alpha_0)^9Be$ below $E_n = 14$ MeV is the absolute measurement of Davis *et al.*[22] shown in Fig. 12. The results of Davis *et al.*[22] are consistent in shape but are smaller in magnitude by approximately a factor of 2 compared with the predicted[23] values of Retz-Schmidt *et al.*[2] and Van der Zwan and Geiger[3] and, by implication, of this experiment.

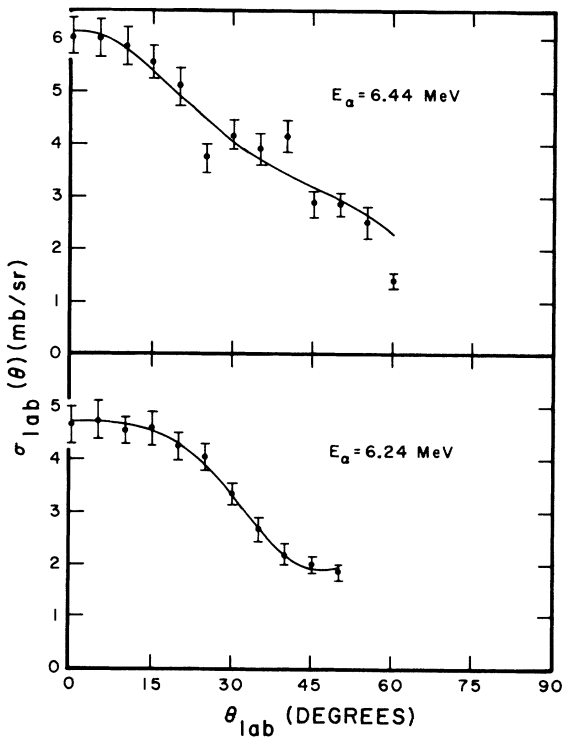

FIG. 11. $^9Be(\alpha, n_3)^{12}C^*_{9.638}$ angular distributions (see caption of Fig. 8).

IV. RESULTS: LOW-ENERGY NEUTRON CONTINUUM

A. Time Spectrum

Above a bombarding energy of 4.8 MeV an apparent neutron continuum was observed at neutron energies less than that of the n_2 group, as shown in Fig. 4(c). The n_3 group, observed above a bombarding energy of 6 MeV, rides on the continuum. It is unlikely that the continuum comes from the broad state in ^{12}C at 10.3-MeV excitation energy, since, as will be discussed in Sec. IV B, the neutron continuum does not exhibit the characteristics of such a state. St. Romain *et al.*[10] and Verbinski *et al.*[20] also find that the continuum is more probably due to a breakup process than to a broad level in ^{12}C.

The other possible reactions producing the continuum are the two sequential decays $^9Be(\alpha, \alpha')^9Be^* \rightarrow {}^8Be + n$ and $^9Be(\alpha, {}^8Be)^5He \rightarrow \alpha + n$ and the two direct processes $^9Be(\alpha, n\alpha)^8Be$ and $^9Be(\alpha, n)3\alpha$. Neutrons have been observed at other laboratories from the decay of the 1.67-, 2.43-, and 3.04-MeV excited states of ^9Be which would be involved with the first of these sequential decays.[1,24] The maximum and minimum neutron energies to be observed from these processes were calculated using the expressions for the kinematics derived by Morinigo[25] for the sequential decays and by Ohlsen[26] for the direct processes. The calculated neutron-energy limits as a function of angle at $E_\alpha = 6.44$ MeV are shown in Fig. 13. The minimum neutron energies for the direct processes are not shown as they are zero for the two cases studied here. The $^9Be(\alpha, {}^8Be)^5He \rightarrow \alpha + n$ process is not shown, since such neutrons would not span enough energy to resemble the data. The sequential breakup limits were calculated assuming that the 1.67-, 2.43-, and 3.04-MeV excited states in ^9Be are sharp states. They have, in fact, widths of 200, 1, and 265 keV, respectively.[27] Inclusion of the finite widths would broaden the allowable energy ranges by about 100 keV each way for the two broad states.

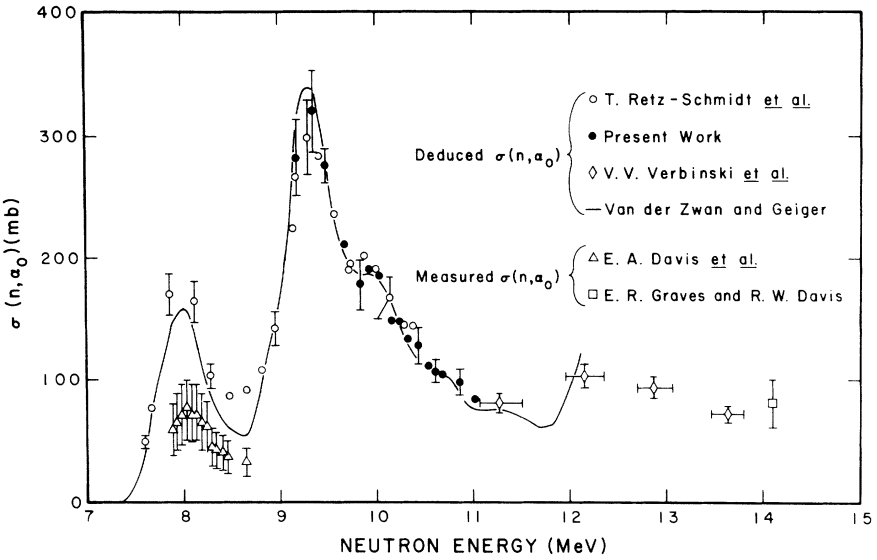

FIG. 12. $^{12}C(n,\alpha_0)^9Be$ angle-integrated cross section. The values deduced from the present work are shown along with the results of Retz-Schmidt *et al.* (Ref. 2), Verbinski *et al.* (Ref. 20), Graves and Davis (Ref. 21), and Davis *et al.* (Ref. 22). Typical absolute errors are shown. The horizontal bars represent the energy spread on target when larger than the data points.

The maximum experimental energies determined from the time spectra agree well with the maximum energies calculated for the sequential process $^9Be(\alpha,\alpha')^9Be^*(3.04)\rightarrow{}^8Be+n$. The overlap region of the 3.04-MeV state minimum energy and the 2.43-MeV state maximum energy might be expected to produce an anomaly in the neutron yield at that neutron energy. The forward-angle neutron yield at the higher bombarding energies does in fact, show a dip, as seen in Fig. 4(c) (channel 250) and also in Fig. 14 (channel 250). Direct breakup, on the other hand, might be expected to produce a smooth curve of neutron yield versus neutron energy. The fact that the experimental energy maxima are slightly higher than the corresponding calculated maxima can be attributed to the 265-keV width of the 3.04-MeV level in ^9Be, which was not included in the calculated energies. The observed maximum energies decrease with decreasing bombarding energy as shown in Fig. 15.

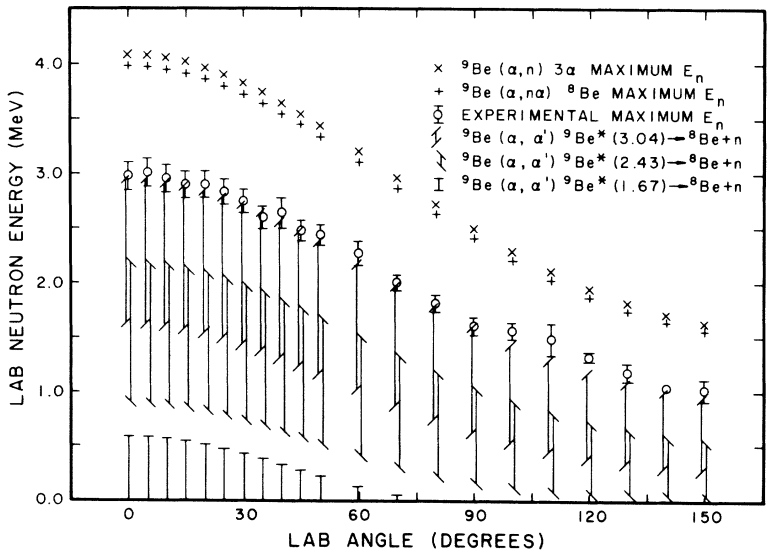

FIG. 13. Neutron-energy limits as a function of angle for the possible many-body-breakup processes from the $^9Be+\alpha$ reaction at 6.44-MeV bombarding energy.

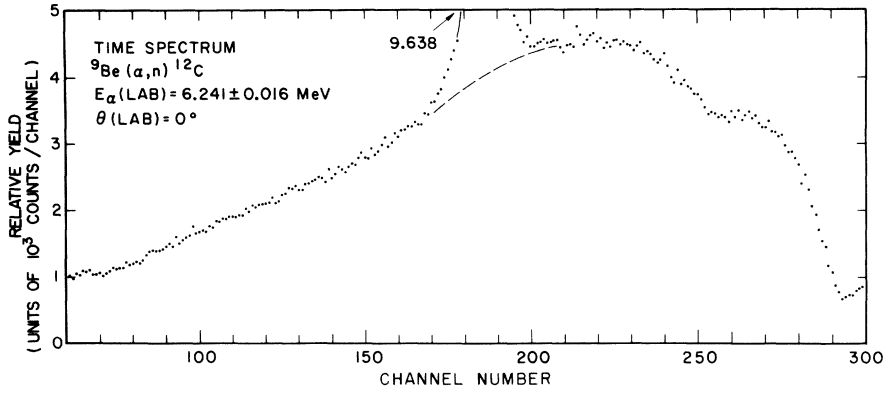

FIG. 14. Time spectrum of continuum neutrons from the $^{9}Be+\alpha$ reaction at 6.24-MeV bombarding energy. The dashed line is a fitted background for the neutron group to the 9.638-MeV level in ^{12}C.

This implies a decreasing population of the 3.04- and then of the 2.43-MeV excited states in ^{9}Be with decreasing bombarding energy. The neutron energy limits as a function of angle at 5.11-MeV bombarding energy are shown in Fig. 16. It can be seen here that over the whole angular range the highest ^{9}Be state excited at this bombarding energy is that at 2.43 MeV. St. Romain *et al.*[10] also found that the continuum neutrons are due to this sequential process, and in fact most such multiparticle processes at low bombarding energies are of the sequential type.[28]

B. Angular Distribution of the Breakup

Breakup cross sections in units of mb/sr MeV were determined by converting the contents of each channel in the continuum region to mb/sr and then dividing the result by the increment in energy between that channel and the next channel. The experimentally determined relation of flight time to channel number was fitted by a quadratic equation (hereafter called the time line) using the known energies of the observed neutron groups. From the time line the energies of the continuum neutrons could then be determined. At the four highest bombarding energies the n_3 group was observed at the forward angles, and a quadratic time line chosen from the spectra which included the n_3 group and which best fitted all the resolved group spectra at that energy was used for all the

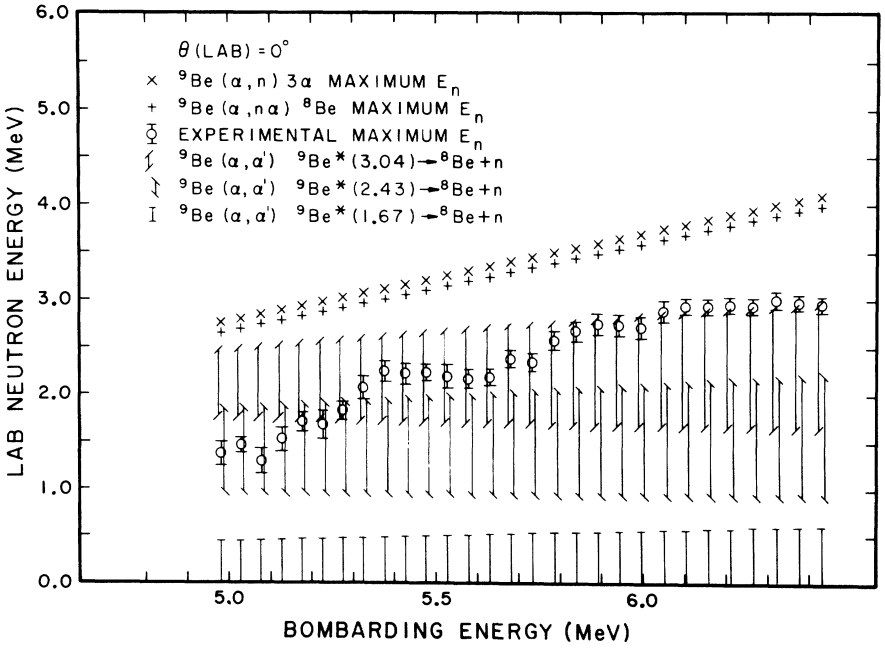

FIG. 15. Neutron-energy limits at 0° as a function of bombarding energy for the possible many-body-breakup processes from the $^{9}Be+\alpha$ reaction.

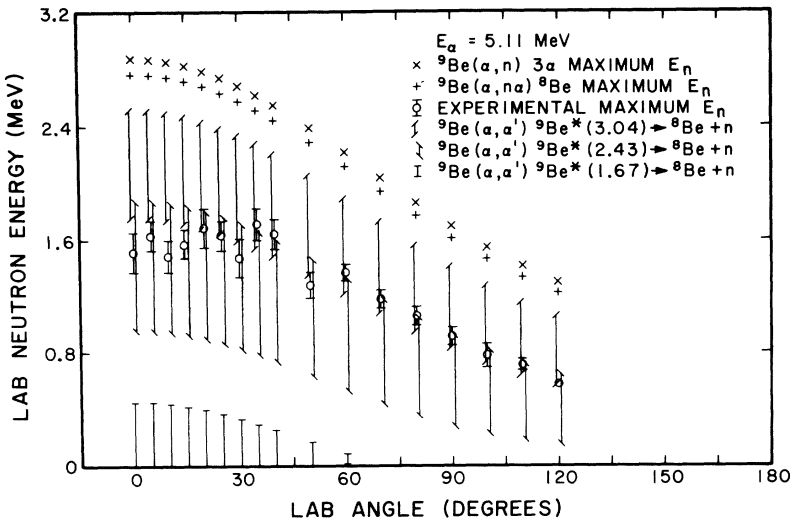

FIG. 16. Neutron-energy limits as a function of angle for the possible many-body-breakup processes from the ^{9}Be+α reaction at 5.11-MeV bombarding energy.

data at that energy. Whenever a time line was applied to a spectrum it was shifted linearly by a time δ nsec calculated from the expression

$$\frac{\partial}{\partial \delta}\left[\sum_{i=1}^{n}\{T_i(\text{experimental}) - [T_i(\text{quadratic}) + \delta]\}^2\right] = 0$$

to take into account possible time shifts between runs. Here T_i is the flight time and n is the number of peaks in a given spectrum. The values of δ were less than 1 nsec most of the time.

The error introduced in extrapolating the time lines to the continuum energies was checked at the highest four bombarding energies by applying time lines generated from only the n_0, n_1, and n_2

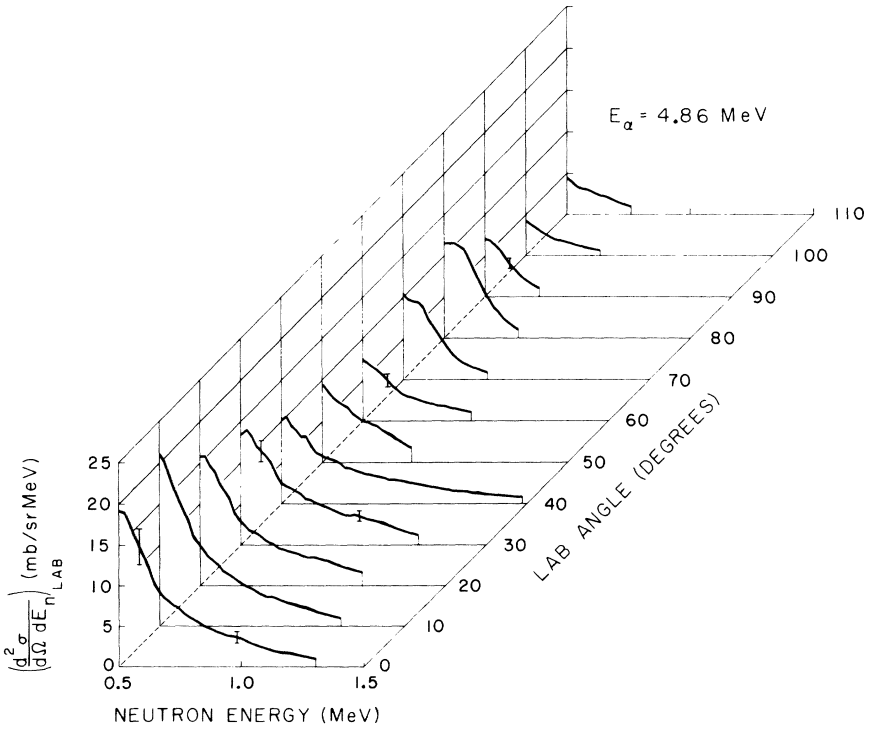

FIG. 17. Continuum angular distribution at 4.86-MeV bombarding energy. The neutron energy in Figs. 17–22 is the laboratory energy and the errors shown are relative to each curve.

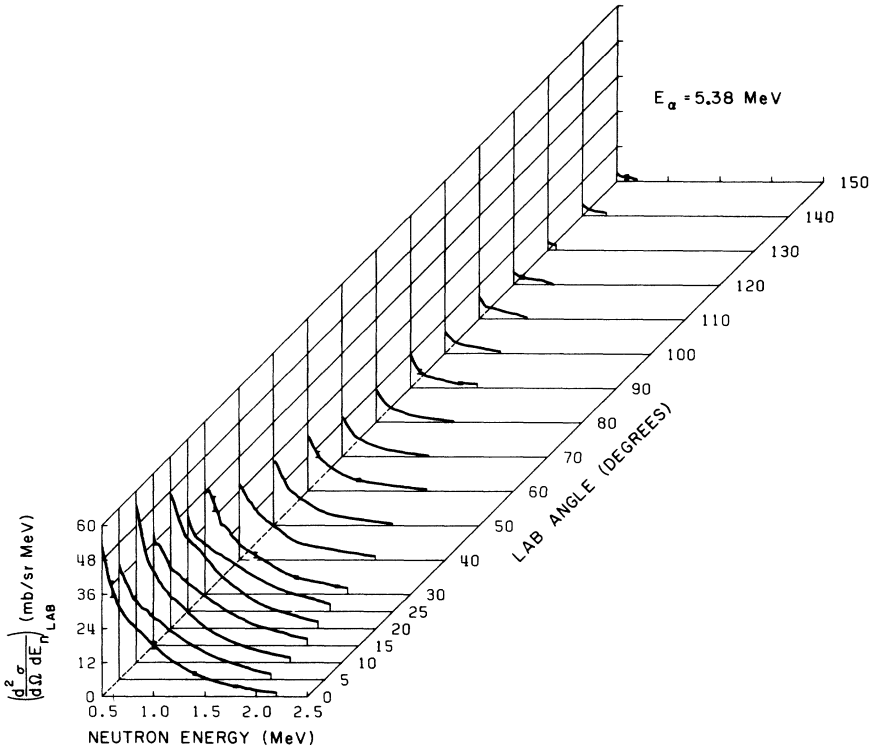

FIG. 18. Continuum angular distribution at 5.38-MeV bombarding energy.

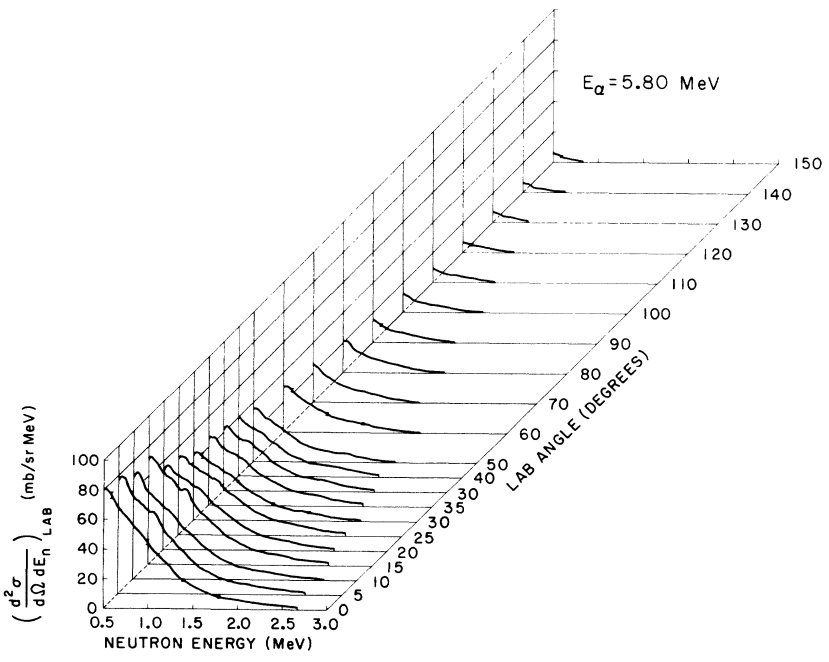

FIG. 19. Continuum angular distribution at 5.80-MeV bombarding energy.

groups to the n_3 groups of all the spectra at that bombarding energy. The deviations of the predicted energy of the n_3 group from the observed energy of the n_3 group were less than ±30 keV.

The continuum was energy-averaged over the width of the detector resolution in order to smooth it. This had no effect on its shape, and was especially desirable at the backward angles and lower bombarding energies where the fluctuations between neighboring channels were large due to low counting statistics.

A linearly varying background was subtracted from the continuum from an energy above the breakup, where the background was clearly visible, down to the low-energy end of the continuum, where it was assumed to be the same as the background above the n_0 group. The backgrounds below the n_2 group and above the n_0 group were, in fact, about the same at bombarding energies below that of the appearance of continuum neutrons. An estimated error associated with making the above choice for the background was folded in with the statistical errors.

10 continuum angular distributions were measured between 4.86- and 6.44-MeV bombarding energy, of which six[29] are shown in Figs. 17 through 22. The cross sections are presented only above 0.5-MeV neutron energy, since the time span on the time-to-amplitude converter was such that neutrons below about 400-keV energy were off the lower end of the time spectrum and therefore could not be seen. Furthermore, the uncertainties in the yields, efficiency, and extrapolated time line were all large below 0.5 MeV, making the cross sections unreliable. The gap seen in Fig. 13 between the energy limits of the 1.67-MeV state neutron group and the 2.43-MeV state neutron group can be seen as an irregular furrow, i.e., a cross section minimum whose position decreases in energy with increasing angle, in the angular distribution at 6.44 MeV (Fig. 22). Such a furrow is thus consistent with the kinematic calculations for sequential decay. It is most prominent at the two highest bombarding energies. This feature cannot be readily seen in the time spectra, because the detection efficiency is changing rapidly for those neutron energies and also because the energy scale for low-energy neutrons is greatly expanded in the time spectra. The furrow does not drop to zero cross section, partly because of the detector resolution and also because of the 200-keV width of the 1.67-MeV state in ^{9}Be which was not included in the kinematic calculations. It is unlikely that the 10.3-

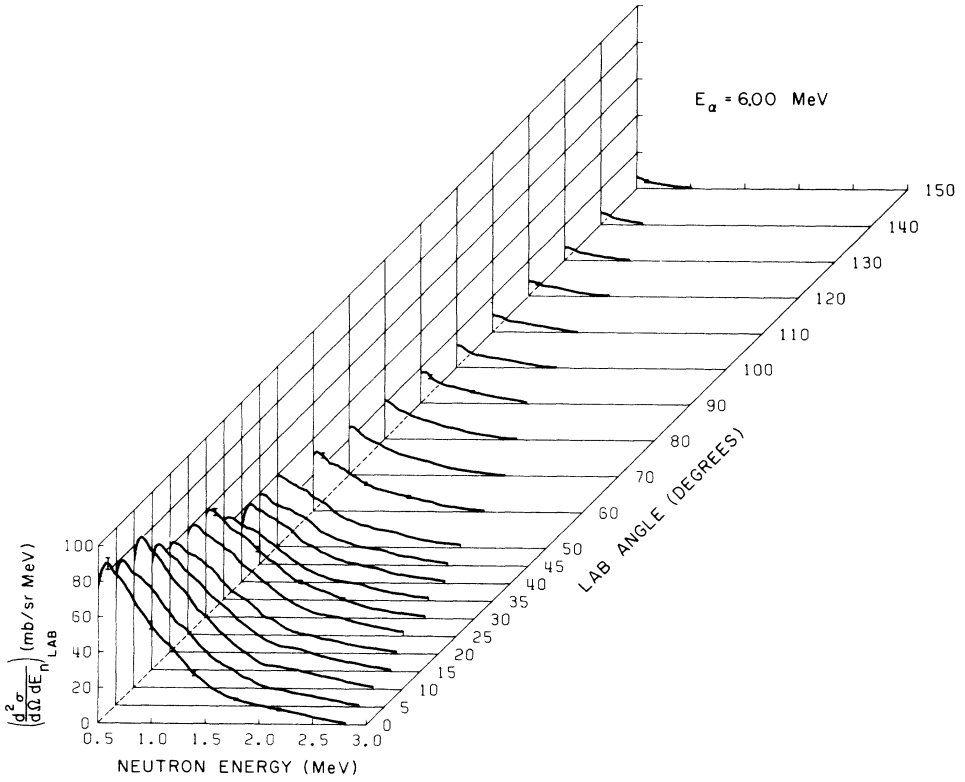

FIG. 20. Continuum angular distribution at 6.00-MeV bombarding energy.

MeV group from ^{12}C contributes appreciably to filling in this gap. Neutrons from such a wide level[1] ($\Gamma = 3.0 \pm 0.7$ MeV) should have a Lorentzian line shape. Assuming that a third of the continuum cross section in the region of the furrow is due to a group populating the 10.3-MeV level, the tail of such a broad group would give a much larger neutron yield in the region of the n_2 group than is experimentally observed. The two distinct slopes in continuum cross section vs neutron energy seen for $E_n > 1$ MeV at bombarding energies greater than 5.8 MeV correspond to the two neutron groups from the 2.43- and 3.04-MeV states in ^{9}Be, respectively. The fact that only one slope is seen for $E_\alpha < 5.8$ MeV is further evidence that the 3.04-MeV state is not populated at the lower bombarding energies.

The breakup cross sections were integrated over angle using the formula

$$\sigma(E_i) = \sum_j \sigma(\theta_j, E_i)\Delta\Omega ,$$

where E_i is the neutron energy in the ith channel. The angle- and energy-integrated cross sections for the breakup neutrons above 0.5-MeV neutron energy are presented in Table I. The sums of the angle-integrated cross sections for the breakup neutrons and for the discrete groups provide the total neutron-production cross section above 0.5-

TABLE I. Total neutron-production cross sections (σ_t) of Gibbons and Macklin (Ref. 4) compared with the present results for $E_n > 0.5$ MeV. The total breakup cross sections (σ_b) measured in the present experiment are also shown. The data for $E_\alpha > 6.44$ MeV in column 3 are the results of Verbinski *et al.* (Ref. 20).

E_α (MeV)	σ_b above 0.5 MeV (mb)	σ_t above 0.5 MeV (mb)	σ_t (Ref. 4) (mb)	Fraction of total >0.5 MeV
4.86	17 ± 3	448 ± 50	400 ± 24	~1
4.98	16 ± 4	477 ± 53	490 ± 29	~1
5.11	25 ± 5	496 ± 55	490 ± 29	~1
5.29	42 ± 8	514 ± 57	540 ± 32	~1
5.38	54 ± 11	557 ± 62	560 ± 34	~1
5.80	130 ± 22	532 ± 60	605 ± 36	0.88
5.90	150 ± 24	506 ± 57	590 ± 35	0.86
6.00	165 ± 26	488 ± 55	570 ± 34	0.86
6.24	204 ± 34	464 ± 55	550 ± 33	0.84
6.44	235 ± 37	453 ± 55	565 ± 34	0.80
6.79		390 ± 39	579 ± 34	0.69
7.96		466 ± 47	660 ± 40	0.71
8.91		535 ± 54	755 ± 45	0.71
9.92		518 ± 52	703 ± 42	0.74

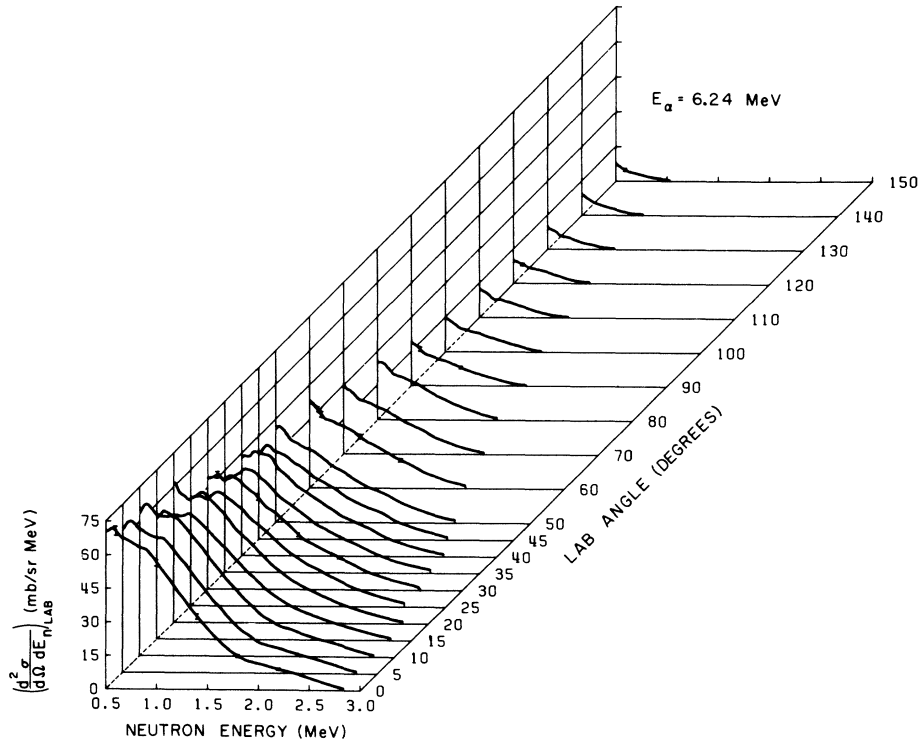

FIG. 21. Continuum angular distribution at 6.24-MeV bombarding energy.

MeV neutron energy. These totals are compared in Table I with the total cross sections found by Gibbons and Macklin[4] using a large graphite sphere detector and also with the total cross sections of Verbinski *et al.*[20] Included in the total cross sections of the present work are the n_3 angle-integrated cross sections, which were estimated to be 1 mb at 5.90 MeV, 5 mb at 6.00 MeV, 10 mb at 6.24 MeV, and 15 mb at 6.44 MeV. The fraction of the total neutron-production cross section which is above 0.5-MeV neutron energy is seen to slowly decrease with increasing bombarding energy, in agreement with the conclusions of Gibbons and Macklin.[4]

V. DISCUSSION

A. Application of the n_0 Group to Neutron Scattering

The largest high-energy neutron yield at 0° can be obtained from the broad peak at about 4.2-MeV bombarding energy which corresponds to 9.8-MeV neutron energy. A second smaller 0° peak at about 5.4-MeV bombarding energy produces neutrons of about 11-MeV energy. A comparison of the neutron fluxes at these two neutron energies with the flux from the reaction $D(d,n)^3He$ for the same energy loss in the target gives the ratios

$$\frac{\sigma(D+d)S(Be+\alpha)}{\sigma(Be+\alpha)S(D+d)} \simeq 56$$

at $E_n = 9.8$ MeV and

$$\frac{\sigma(D+d)S(Be+\alpha)}{\sigma(Be+\alpha)S(D+d)} \simeq 326$$

at $E_n = 11$ MeV. Here σ is the 0° differential cross section[15] and S is the atomic-stopping cross section.[17] Two considerations tend to compensate for the small flux from the reaction $^9Be(\alpha,n)^{12}C$. The first is that solid beryllium targets can easily be used having much larger energy spreads than gaseous deuterium targets. This not only decreases the above ratios because of the larger relative number of target atoms per square centimeter, but can also be useful in averaging over fluctuations present in the neutron-scattering excitation functions. The second consideration is that the incident deuterons in the above ratios have bombarding energies of 6.6 and 7.9 MeV, respectively, and these energies are often not readily available to low-energy accelerators. The use of a high-efficiency detector such as the 5-in.×5-in. liquid scintillator used in the present experiment can make neutron-scattering experi-

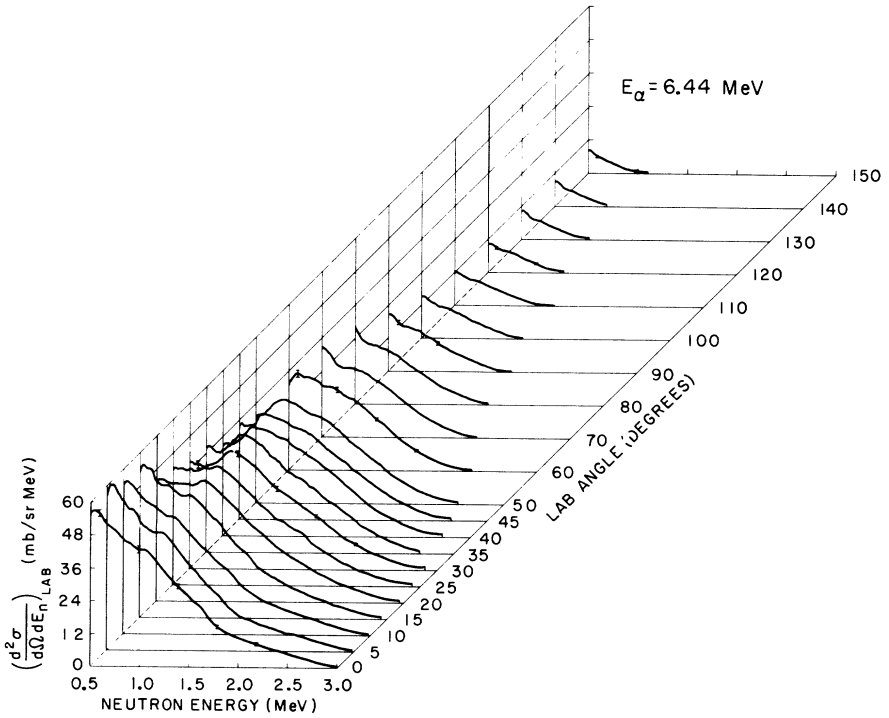

FIG. 22. Continuum angular distribution at 6.44-MeV bombarding energy.

ments with the source reaction $^9Be(\alpha,n)^{12}C$ quite feasible.

As a source of high-energy polarized neutrons, the reaction $^9Be(\alpha,n)^{12}C$ compares more favorably with the reaction $D(d,n)^3He$. In this case the quantity of interest is $P^2\sigma/S$, where P is the magnitude of the polarization of the neutrons emitted in the reaction, σ is the differential cross section of the reaction, and S is the atomic-stopping cross section of the target material.[17] The larger the magnitude of this quantity, the smaller is the uncertainty that results in the measured asymmetry in a double scattering experiment. The maximum values of $P^2\sigma/S$ are tabulated as a function of E_n in Table II. The $D(d,n)^3He$ polarizations were taken from Haeberli[30] and Niewodniczanski, Szmider, and Szymakowski,[31] while the $^9Be(\alpha,n_0)^{12}C$ polarizations were obtained from Donoghue.[32] The $D(d,n)^3He$ cross sections were obtained by interpolating the cross sections of Brolley and Fowler.[14] Again the use of beryllium targets with much larger numbers of target atoms per square centimeter than are easily obtainable with deuterium gas targets could enhance the values of $P^2\sigma/S$ relative to the $D(d,n)^3He$ values by a factor of up to 10.

B. Astrophysical Implications

In the interior of red giant stars, it is believed that the resonance reaction

$$3\alpha \rightarrow {}^8Be + \alpha \rightarrow {}^{12}C^*_{7.65} \rightarrow {}^{12}C + \gamma$$

is the first stage of helium burning. The ^{12}C nucleus in its second excited state can decay to the entrance channel, to the first excited state of ^{12}C, or to the ground state of ^{12}C. The probability of the decay of the 0^+ level in ^{12}C at 7.656-MeV excitation energy directly to the 0^+ ground state of ^{12}C was measured using the reaction $^9Be(\alpha,n)^{12}C$ to populate the excited states of ^{12}C. This was done by Alburger,[11] who measured the ratio of the number of 7.656-MeV $E0$ nuclear pairs to the number of internal-conversion pairs from the 4.439-MeV $E2$ γ ray deexciting the first excited state. Combining this quantity with the ratio of initial populations of the two levels, one can determine the ratio of the width of the 7.656-MeV level for pair emission to the total width of the level ($\Gamma_{e^\pm}/\Gamma$). The ratio of level population as a function of bombarding energy, i.e., of the yield

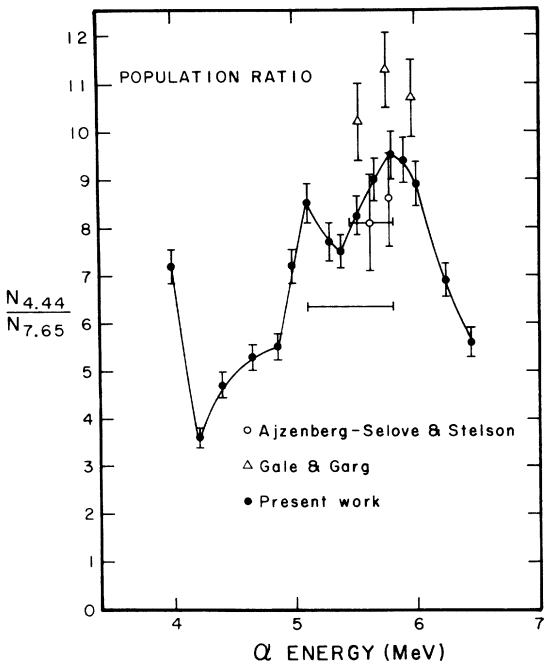

FIG. 23. Relative population of the first and second excited states in ^{12}C produced by the reaction $^9Be(\alpha,n)^{12}C$ from the present work. The data of Ajzenberg-Selove and Stelson (Ref. 5) and Gale and Garg (Ref. 19) are also presented. The total errors in the ratios are shown. The horizontal bars represent the energy spread on target when larger than the data points. The single horizontal bar indicates the energy loss in Alburger's thin target (see Ref. 11).

TABLE II. Comparison of the maximum figure of merit $P^2\sigma/S$ for the reactions $^9Be(\alpha, n_0)^{12}C$ and $D(d, n)^3He$ at the same neutron energies.

		$^9Be(\alpha, n_0)^{12}C$			$D(d, n)^3He$		$P^2\sigma/S$	
E_n (MeV)	E_α (MeV)	θ_{lab} (deg)	Pol.[a]	E_d (MeV)	θ_{lab} (deg)	Pol.[b]	$^9Be(\alpha, n_0)^{12}C$	$D(d, n)^3He$
7.6	5.25	115	0.70	5.4	33	0.08	0.13	0.09
8.0	5.50	110	0.55	5.9	33	0.10	0.09	0.13
9.0	4.50	60	0.45	7.1	32	0.16	0.07	0.35
9.4	5.85	75	0.65	7.6	32	0.18	0.05	0.42
10.3	5.00	30	0.50	8.7	32	0.23	0.43	0.68
10.7	5.25	20	0.45	9.2	32	0.24	0.30	0.78
10.9	5.50	20	0.35	9.4	32	0.25	0.20	0.86

[a] Reference 32.

[b] References 30 and 31.

of the n_1 to the n_2 group, R, measured in the present experiment is shown in Fig. 23. The data of Azjenberg-Selove and Stelson[5] and Gale and Garg[19] are also presented. The single horizontal bar indicates the energy loss in Alburger's thin target,[11] upon which his results are based. The average value of the six ratios measured in the present experiment over the energy range of Alburger's thin target is $\bar{R} = 8.4 \pm 0.4$. A more accurate determination of the nuclear-pair-decay probability of the 7.656-MeV state in ^{12}C still awaits a more accurate measurement of the ratio of $E0$ to $E2$ pairs, which in Alburger's[11] experiment was measured to ±30%. Combining the present value for R with Alburger's pair intensity ratio gives

$$\Gamma_{e^\pm}/\Gamma = 8.2 \times 10^{-7} \times 8.4 = (6.9 \pm 30\%) \times 10^{-6}.$$

Our accurate measurement of R, together with the Alburger data, does make the 0^+ assignment of the 7.65-MeV state more certain.

ACKNOWLEDGMENTS

The authors wish to thank Professor M. T. McEllistrem and Professor J. D. Brandenberger for many helpful discussions during the course of this work, and Dr. W. Galati for assistance in the early phases of the experiments. The assistance of the technical staff is greatly appreciated. We also wish to thank the University of Kentucky Computing Center for their cooperation and for providing computer time for data reduction and analysis.

---

*Work supported in part by a grant from the National Science Foundation.

†Work performed in partial fulfillment of the requirements for the Ph.D. degree. Present address: Florida State University, Tallahassee, Florida.

‡Present address: University of Windsor, Windsor, Ontario.

§Presently on leave at Rutherford High Energy Laboratory, Chilton, Didcot, Berkshire, England.

[1]F. Ajzenberg-Selove and T. Lauritsen, Nucl. Phys. A114, 1 (1968).

[2]T. Retz-Schmidt, T. W. Bonner, G. U. Din, and J. L. Weil, Bull. Am. Phys. Soc. 5, 110 (1960); J. L. Weil, private communication.

[3]L. Van der Zwan and K. W. Geiger, Nucl. Phys. A152, 481 (1970).

[4]J. H. Gibbons and R. L. Macklin, Phys. Rev. 137, B1508 (1965).

[5]F. Ajzenberg-Selove and P. H. Stelson, Phys. Rev. 120, 500 (1960).

[6]T. W. Bonner, A. A. Kraus, Jr., J. B. Marion, and J. P. Schiffer, Phys. Rev. 102, 1348 (1956).

[7]J. R. Risser, J. E. Price, and C. M. Class, Phys. Rev. 105, 1288 (1957).

[8]R. G. Miller and R. W. Kavanagh, Nucl. Phys. 88, 492 (1966).

[9]Ajzenberg-Selove and Stelson (Ref. 5) give numbers from which the angle-integrated n_2 yield at $E_\alpha = 5.78$ MeV can be calculated.

[10]F. A. St. Romain, T. W. Bonner, R. L. Bramblett, and J. Hanna, Phys. Rev. 126, 1794 (1962).

[11]D. E. Alburger, Phys. Rev. 118, 235 (1960).

[12]J. B. Marion, Rev. Mod. Phys. 38, 660 (1966).

[13]J. D. Reber and J. D. Brandenberger, Phys. Rev. 163, 1077 (1967). Only the larger shield illustrated in this reference was used.

[14]J. E. Brolley, Jr., and J. L. Fowler, *Fast Neutron Physics*, (Interscience, New York, 1960), Pt I, p. 73.

[15]M. D. Goldberg, private communication.

[16]V. V. Verbinski, J. C. Courtney, W. R. Burrus, and T. A. Love, Oak Ridge National Laboratory Report No. ORNL-P-993, 1964 (unpublished).

[17]W. Whaling, in *Handbuch der Physik*, edited by S. Flügge (Springer, Berlin 1958), Vol. 34.

[18]Tables of coefficients from Legendre-polynomial fits to the angular distributions are available from the authors.

[19]N. H. Gale and J. B. Garg, Nuovo Cimento 19, 742 (1961).

[20]V. V. Verbinski, F. G. Perey, J. K. Dickens, and W. R. Burrus, Phys. Rev. 170, 916 (1968).

[21]E. R. Graves and R. W. Davis, Phys. Rev. 97, 1205 (1955).

[22]E. A. Davis, T. W. Bonner, D. W. Worley, Jr., and R. Bass, Nucl. Phys. 48, 169 (1963).

[23]The reciprocity relation $\sigma(\alpha,n)(2I_1+1)M_\alpha E_\alpha = \sigma(n,\alpha) \times (2I_2+1)M_n E_n$ was used. $I_1 = \frac{3}{2}$, $I_2 = \frac{1}{2}$, M_α and M_n are reduced masses, and E_α, E_n are in the center-of-mass system.

[24]Y. S. Chen, Bull. Am. Phys. Soc. 15, 1688 (1970).

[25]F. B. Morinigo, Nucl. Phys. A127, 116 (1969).

[26]G. G. Ohlsen, Nucl. Instr. Methods 37, 240 (1965).

[27]F. Ajzenberg-Selove and T. Lauritsen, Nucl. Phys. 78, 1 (1966).

[28]H. D. Holmgren, in *Nuclear Research with Low Energy Accelerators*, (Academic, New York, 1967), p. 213.

[29]The remaining four continuum angular distributions are fairly similar to those shown at neighboring energies. Graphs of this unpublished data are available from the authors.

[30]W. Haeberli, University of Wisconsin Report No. TID-18137, 1963 (unpublished).

[31]H. Niewodniczanski, J. Szmider, and J. Szymakowski, Institute of Nuclear Physics, Krakow, Report No. PAN-262, 1963 (unpublished).

[32]D. C. DeMartini, C. R. Soltesz, and T. R. Donoghue, to be published.